International Journal of Fracture **115:** 205–226, 2002.

Determination of the Fracture Toughness of a Low Alloy Steel by the Instrumented Charpy Impact Test

A. ROSSOLL*, C. BERDIN and C. PRIOUL
Laboratoire de Mécanique des Sols, Structures et Matèreaux, École Centrale de Paris, Grande Voie des Vignes, F-92295 Châtenay-Malabry Cedex, France (e-mail: andreas.rossoll@epfl.ch)

Received 22 February 2001; accepted in revised form 27 August 2001

Abstract. An attempt to establish a non-empirical relationship between the Charpy V-notch energy *CVN* and the fracture toughness K_{Ic} is presented. We focus our study on the lower shelf of fracture toughness and on the onset of the ductile-to-brittle transition of a A508 Cl.3 low alloy structural steel. The methodology employed is based on the 'local approach'. Brittle cleavage fracture is modelled in terms of the Beremin (1983) model, whereas the ductile crack advance preceding cleavage in the transition region is accounted for with the GTN model (Gurson, 1977; Tvergaard, 1982; Tvergaard and Needleman, 1984. Mechanical testing at different strain rates and temperatures allowed the establishment of the constitutive equations of the material in a rate dependent formulation. Numerous fracture tests on different specimen geometries provided the large data set necessary for statistical evaluation. All specimen types were modelled with finite element analysis. Special consideration was taken in order to handle the dynamic effects in the Charpy impact test in an appropriate way. The fracture toughness could be predicted from Charpy impact test results, on the lower shelf, by applying the 'local approach'. In the transition region the parameters of the Beremin model were found to deviate from those established on the lower shelf. Detailed fractographic investigations showed that the nature of 'weak spots' inducing cleavage fracture changes with temperature. It is concluded that the Beremin model must be refined in order to be applicable in the ductile-to-brittle transition region.

Key words: Charpy test, cleavage fracture, ductile damage, fractography, fracture toughness, local approach, numerical modelling.

1. Introduction

The Charpy impact test has been used for the toughness assessment of metallic materials for one hundred years. It is standardized and largely applied in industry, due to the simple, rapid and inexpensive testing procedure. Charpy impact testing is largely employed for characterizing a material's DBTT (ductile-to-brittle transition temperature). However, it cannot directly be used for *quantitative* safety assessment by the means of fracture mechanics, since *CVN* (Charpy impact energy) and K_{Ic} (fracture toughness) are not directly related. This is rather obvious, since these two measures are fundamentally different:

- The fracture toughness K_{Ic} is defined as the critical stress intensity factor and it denotes a material's resistance to the propagation of an (already existing) crack.
- The Charpy impact energy *CVN* contains both crack propagating energy as well as the energy necessary for crack initiation, since the standard Charpy V-notch specimen is not provided with a pre-crack. These two principal (as well as a few minor) contributions to the overall energy consumed during a test cannot be separated.

*Current affilation: Laboratoire de Métallurgie Mécanique, Département des Matériaux, École Polytechnique Fédérale de Lausanne, CH-1015 Lausanne, Switzerland

In our work we attempt to establish a non-empirical relationship between *CVN* and K_{Ic}, for an A508 Cl.3 low alloy construction steel. The domain of interest is the lower shelf of fracture toughness (up to K_{Ic} values on the order of some 100 MPa$\sqrt{m}$). This region is situated at low temperature, where the dominant failure mode is cleavage fracture. An attempt to predict the fracture toughness on the onset of the ductile-to-brittle transition is also made.

Numerous procedures have been developped in the past, aiming at converting *CVN* to K_{Ic} values, based on empirical formulas. Server (1985) and Hertzberg (1995) provide compilations of these correlations. On the lower shelf of fracture toughness, basically the following two types of approaches can be distinguished: the simplest correlations convert *CVN* to K_{Ic} in one step (Barsom and Rolfe, 1970; Sailors and Corten, 1972; Barsom, 1975), whereas slightly more elaborated ones (Marandet and Sanz, 1977; Wallin, 1989) require accounting for the difference in DBTT between *CVN* and K_{Ic} via a shifting procedure. However, a less empirical conversion would be desirable, since the degree of conservatism given by these correlations depends strongly on the material, and no unique correlation can cover the entire transition range.

More quantitative information from the Charpy test can be acquired by instrumentation of the striker (e.g., with strain gauges) such that load vs. time or load vs. loadline displacement (deflection) records are obtained. Evaluation of the general yield load allows the estimation of the (dynamic) yield stress (Fearnehough and Hoy, 1964; Server, 1978a, 1978b). Simple analytical estimations of the fracture stress can also be made, if fracture occurs prior to or at general yield (Fearnehough and Hoy, 1964; Wilshaw and Pratt, 1966; Knott, 1967; Wullaert, 1970).

A further step towards a more quantitative assessment is the use of *pre-cracked* specimens. Pre-cracking up to a notch depth ratio *a/W* of about 0.55 adapts the Charpy specimen geometry to the application of fracture mechanics. Standards (ESIS, 1996a,b) are in the course of development that will allow the application of pre-cracked Charpy specimens for (dynamic) fracture mechanics (K_{Id}, J_{Id}, CTOD, CTOA) evaluation. However, it can be anticipated that validity problems will be encountered. The small size of the Charpy specimen leads to general yielding very early in the loading history. Furthermore, in order to monitor the irradiation-induced embrittlement of components used in the nuclear industry, *standard* (not pre-cracked) Charpy V-notch specimens are currently used, which cannot easily be pre-cracked before testing.

A methodology that could allow the development of a better founded procedure for the exploitation of the Charpy V-notch test is promised by the 'local' approach. In contrast to the 'global' approach based on the application of fracture mechanics, as described above, the 'local' approach is based on the direct examination of some local field quantities, that appear to control damage evolution and fracture initiation for the fracture type to be examined. The computation of these local parameters is commonly carried out by means of FEM (finite element method). The application of the local approach is based on the following steps (Mudry, 1987): (1) establishment of a model that captures the physical mechanism of the damage or fracture phenomenon, and (2) computation of the relevant field variables, e.g. by FEM. Since the fracture criterion is only material dependent, the parameters of the model should be independent of the specimen geometry.

This approach was applied in this study. Tensile and compressive tests served to establish the constitutive behaviour of the material, which is needed as an input for modelling. The tests were run over a large range of temperatures and strain rates. Fracture was studied on notched tensile (NT), compact tension (CT) and Charpy V-notch (CVN) specimens. The presentation of these experimental results is followed by the description of the FEM modelling

Table 1. Chemical composition (in weight percent)

C	S	P	Mn	Si	Ni	Cr	Mo	Cu	Al
0.159	0.008	0.005	1.37	0.24	0.70	0.17	0.50	0.06	0.023

methodology. In the case of the Charpy test, the definition of a suitable modelling procedure required the examination of the dynamic effects that are characteristic for this type of test. We then present our attempt to predict the fracture toughness from Charpy test results, by the combination of micromechanistically based models of ductile crack growth and cleavage failure (local approach). Finally, on the basis of an extensive fractographic analysis, some implications on eventual modifications of the Beremin model are discussed.

2. Experimental procedures

2.1. Material flow stress

The studied material is a low alloy structural steel of French standard 16MND5 (similar to A508 Cl.3), as it is typically used for heavy section forgings of pressure vessels. The samples were taken at $\frac{3}{4}$ thickness (from the inner wall) from a nozzle cut-out of a pressure vessel. The chemical composition is given in Table 1.

The heat treatment includes two austenitisations followed by water quench and tempering, and a final stress relief treatment. The resulting microstructure is tempered bainite.

A detailed analysis of the non-metallic inclusions was carried out by Renevey (1997). Image analysis on polished surfaces yielded a mean inclusion volume fraction of $f_v = 9.4 \times 10^{-4}$ (mainly manganese sulfides and oxides). This value can be compared to $f_v = 3.9 \times 10^{-4}$ as given by the Franklin (1969) formula for the inclusion volume fraction of manganese sulfides, or $f_v = 5.7 \times 10^{-4}$ if oxides are also considered. The mean dimension of inclusions was 10 ± 2 μm (slightly ellipsoidal).

Tensile tests on smooth specimens were run on a servohydraulic testing machine at a nominal strain rate $\dot{\epsilon}$ of 4×10^{-4} s^{-1} at temperatures ranging from -150 °C up to room temperature (Renevey, 1997). Compressive tests at a strain rate of approximately 1000 s^{-1} were conducted at CREA (Centre de Recherche et d'Études d'Arcueil) on a Hopkinson bar device (Rossoll, 1998). Specimens of cylindrical section of relatively small size (4 mm height, 5 mm diameter) were employed, in order to minimize friction and inertia effects. Rapid testing does not allow for heat transfer to take place and can be regarded as 'adiabatic'. In order to obtain the material flow curve under virtually 'isothermal' conditions, only the plastic deformation up to an amount of 5% was considered. Additional quasistatic (4×10^{-3} s^{-l}) and intermediate strain rate (1 s^{-l}) compressive tests were carried out on a servohydraulic testing machine at CREA as well, at temperatures between -150 °C and $+100$ °C (Rossoll, 1998).

2.2. Fracture tests

Axisymmetric notched tensile bars denominated 'NT2' (6 mm net section, 1.2 mm notch root radius) and 'NT4' (6 mm net section, 2.4 mm notch root radius) were tested on a servohy-

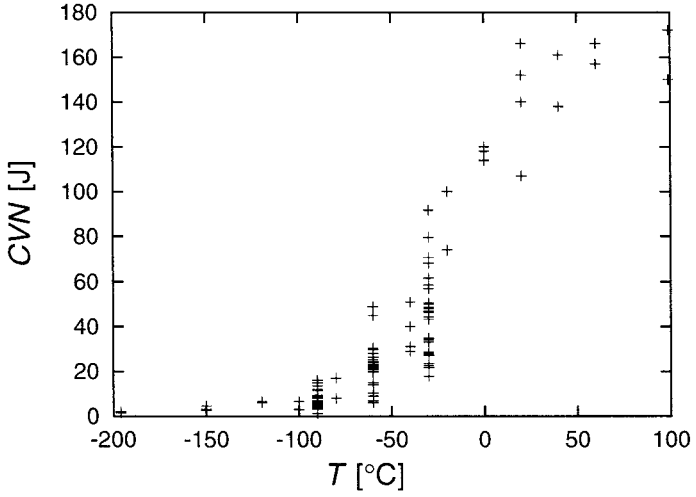

Figure 1. Charpy impact energy as a function of temperature.

draulic testing machine at a crosshead speed of 0.25 mm min^{-1} (Renevey, 1997). The testing temperature was −150 °C for the NT2 specimens, and −90 °C for the NT4 specimens.

Charpy tests were carried out on four different standard instrumented impact pendulum devices of capacities ranking from 100 J up to 350 J, at impact velocities between 5 and 5.5 ms^{-1} and temperatures ranging from −90 °C up to room temperature (Rossoll, 1998). The entire *CVN* transition curve (including some results from Renevey, 1997) is given in Figure 1. Note that at each temperature −90 °C, −60 °C and −30 °C some 30 data points are available. The lower shelf energy level is situated around 5 J, whereas the upper shelf is about 160 J.

Twenty-five mm wide CT specimens with a notch depth ratio *a/W* of 0.55 were tested on the same testing machine and cooling device as employed for the tests on the tensile and notched tensile specimens. A crosshead velocity of 0.5 mm min^{-l} was imposed. The tests were run in the temperature range between −150 °C and −60 °C. Twenty-four specimens were tested at −90 °C. Additional data obtained by Renevey (1997) at −30 °C and 0 °C were also analysed.

Figure 2 shows the fracture surface of a CVN specimen tested at $T = -30°$ C. Several observations that are typical for specimens tested in the transition region can be made. First, the lateral contraction of the specimen is important. Secondly, the shape of the ductile crack zone is very irregular. The material is not capable of sustaining the large strain occurring in the notch root area, which induces numerous secondary ductile cracks. Finally, the macroscopic pattern of ridges that form a sort of 'fan' on the cleavage fracture surface indicates the presence of the cleavage initiation site(s).

3. Numerical Modelling

3.1. Constitutive equations

The mechanical tests conducted at different strain rates and different temperatures served to determine the rate and temperature dependent flow stress of the material. Since ductile crack initiation and propagation occurs in some of the fracture tests, a model incorporating ductile damage has to be chosen for modelling. Here the GTN model for a porous plastic solid,

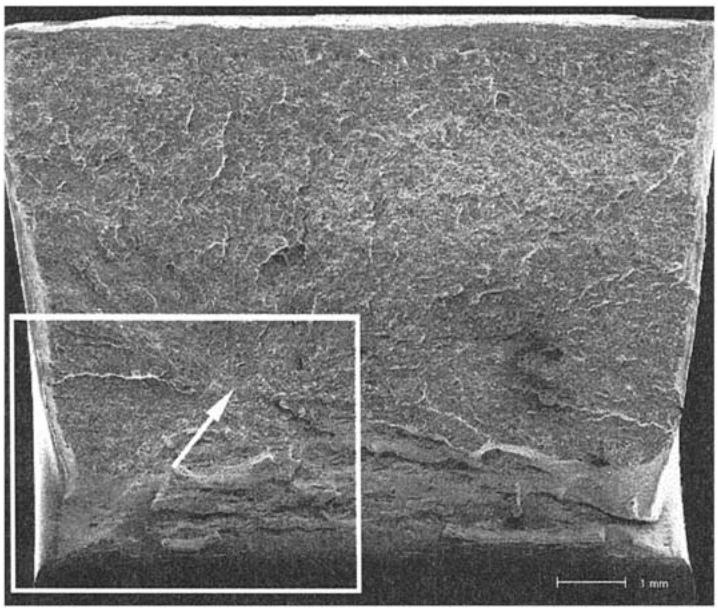

Figure 2. SEM photograph of a CVN specimen fractured at $T = -30$ °C with a *CVN* of 91 J (corresponding to a deflection d of 5 mm). The arrow points to the region where cleavage fracture was triggered. The significance of the white framed box is explained in the legend of Figure 5.

originally proposed by Gurson (1977) and subsequently modified (Tvergaard, 1981, 1982; Tvergaard and Needleman, 1984) was used. The flow potential reads

$$\Phi = \left(\frac{\sigma_{\text{eq}}}{\bar{\sigma}}\right)^2 + 2q_1 f^* \cosh\left(\frac{3q_2}{2}\frac{\sigma_h}{\bar{\sigma}}\right) - (1 + q_1^2 f^{*2}) = 0 \tag{1}$$

with

$$f^* = \begin{cases} f & \text{for } f \le f_c \\ f_c + \kappa(f - f_c) & \text{for } f > f_c \end{cases} \tag{2}$$

where σ_{eq} is the macroscopic effective von Mises stress; σ_h, macroscopic hydrostatic stress; $\bar{\sigma}$, current flow stress of the (fully dense) matrix; f, void volume fraction; q_1, q_2, parameters commonly set to 1.5 and 1, respectively; $\kappa = (1/q_1 - f_c)/(f_f - f_c)$; f_c, critical void volume fraction; f_f, void volume fraction at fracture.

The evolution of the void volume fraction is partly due to growth of existing voids and partly due to nucleation of new voids. The latter is assumed to follow a Gaussian law as suggested by Chu and Needleman (1980) and approved by Kwon and Asaro (1990):

$$\dot{f} = (1 - f)\dot{\epsilon}_{ij}^{\text{pl}}\delta_{ij} + \frac{f_N}{s_N\sqrt{2\pi}} \exp\left[-\frac{1}{2}\left(\frac{\epsilon_M^{\text{pl}} - \epsilon_N}{s_N}\right)^2\right]\dot{\epsilon}_M^{\text{pl}}, \tag{3}$$

where $\dot{\epsilon}_{ij}^{\text{pl}}$ is the plastic part of the macroscopic strain increment, δ_{ij} the Kronecker delta, $\dot{\epsilon}_M^{\text{pl}}$ the equivalent plastic strain increment in the matrix, f_N is the volume fraction of void nucleating particles, ϵ_N the mean strain for nucleation, and s_N the corresponding standard deviation.

For modelling the rate dependence of the flow stress $\bar{\sigma}$ of the matrix, a Cowper–Symonds (Bodner and Symonds, 1960; Perzyna, 1963) overstress formulation was used

$$\bar{\sigma} = \sigma_0 \left(1 + \left(\frac{\dot{\epsilon}_{\text{eq}}}{\dot{\epsilon}_0} \right)^{1/p} \right), \tag{4}$$

where $\bar{\sigma} = \bar{\sigma}(\epsilon_M^{\text{pl}}, \dot{\epsilon}_{eq}, T)$, dynamic flow stress; $\sigma_0 = \sigma_0(\epsilon_{\text{pl}}, T)$, static flow stress; $\dot{\epsilon}_{\text{eq}}$, equivalent plastic strain rate; $\dot{\epsilon}_0 = \dot{\epsilon}_0(T)$, normalisation parameter; $p = p(T)$, strain rate hardening parameter.

The 'static' plastic flow stress σ_0 is assumed to follow a Hollomon law, with a linear dependence on the temperature for the range between -90 °C and $+100$ °C:

$$\sigma_0 = K \left(\epsilon_M^{\text{pl}} \right)^n \left[1 - \beta \left(T - T_0 \right) \right] \tag{5}$$

where $T_0 = -90$ °C, $\beta = 0.00125$, $K = 1040$, MPa and $n = 0.14$. Above $+100$ °C the flow stress is assumed to remain constant (i.e., no further softening occurs with temperature).

The constitutive equations were implemented into the ABAQUS/Standard general purpose finite element program (HKS, 1997) via a user interface as a 'user material' by Siegmund and Brocks (1997) and Mühlich et al. (1998).

The initial volume fraction of voids f_0 was chosen as the average of the two values given by Franklin 's formulas, i.e., $f_0 = 0.005$. Following Fisher and Gurland (1981) who stated that only 10–40% of the carbides give rise to void nucleation, the volume fraction of voids created by nucleation, f_N was taken as 25% of the Fe_3C carbides present (under the assumption that the entire carbon content of the material is present in the form of Fe_3C). Standard values were chosen for the remaining nucleation parameters, i.e, $\epsilon_N = 0.3$ and $s_N = 0.1$. A value of 4 was chosen for the void growth acceleration factor κ which guarantees a good simulation of the load drop in tensile test simulations, and also assures good numerical convergence. Only two parameters were actually fitted, in order to achieve a good simulation of global load-displacement curves. The critical void volume fraction f_c was identified by simulation of smooth tensile tests; $f_c = 0.06$ allowed a good prediction for the occurrence of necking.

A parametric study on the crack growth rate in CT specimens yielded 100 μm as an appropriate value for the size of the dimension of the finite elements in the direction of the strongest stress and strain gradients. This element size was also used in the notch area of the Charpy specimen. Linear elements with selectively reduced integration were employed, since they offered good performance in situations of extensive plastic flow and damage. CVN, as well as CT, specimens were modelled with 3-D elements, whereas axisymmetric elements were used for the tensile bars.

In the case of the Charpy impact test, some additional difficulties are encountered in modelling. Above all, questions arise on 1) the importance of dynamic (inertial) effects; 2) the influence of the high strain rate (strain rate sensitivity and adiabatic heating); 3) the state of constraint in the small size specimen; 4) the complexity of boundary conditions. FEM computations aiming at the examination of mechanical aspects of the Charpy impact test have been presented by Ayres (1976), Norris (1979), Tvergaard and Needleman (1988), Nakamura et al. (1989), Mathur et al. (1993), amongst others. Marur (1996) simulated large impact specimens. However, comparisons between model and experiment are still rare.

3.2. Charpy test modelling

We conducted a preliminary study (Rossoll, 1998; Rossoll et al., 1999) in order to define a modelling procedure that would be appropriate for the local approach. The employed methods

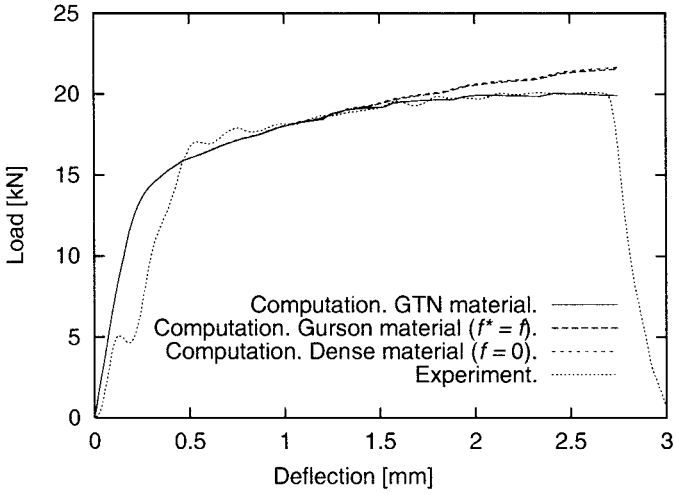

Figure 3. Comparison of load-displacement curves obtained with different numerical models (3-D), and an experimental record. $T = -60\ ^{\circ}\mathrm{C}$. Note that the apparent delay of the rise of the experimental load signal is an artefact due to excessive electronic filtering (low cut-off frequency) in the testing apparatus employed, as was shown in Rossoll (1998).

were quasistatic (2-D and 3-D), transient dynamic (2-D) and modal (2-D) FEM, as well as analytic analysis. Our principal findings are:

(1) Inertial oscillations of the experimental load vs. displacement curves originate from the vibration of the specimen. Whereas the specimen can be considered, in a first approximation, as a (free) Timoshenko beam, a more precise analysis requires taking into account its contact with the striker. Compliance of the striker (which in general is deliberately constructed as strongly compliant in order for the attached strain gages to yield high output) strongly influences the frequency of specimen vibrations. Local stress fluctuations inside the specimen (ahead of the notch root) are much less important. For the range of loading durations greater than 50 μs (corresponding to the lowest *CVN* values obtained at $-90\ ^{\circ}\mathrm{C}$) a quasistatic procedure is sufficient for the interpretation of experimental results, as well as for modelling.

(2) The high strain rate ($\dot{\epsilon} \sim 10^3\ \mathrm{s}^{-1}$) in the notch root of the Charpy specimen needs to be accounted for via a strain rate dependent material law. Adiabatic heating is important. However, its effect is confined to the notch root, and does not strongly lower the level of the maximum stress.

(3) A 2-D plane strain model is sufficient to describe the local stress and strain fields ahead of the notch, as long as no ductile crack growth occurs. The global response (load) is, not surprisingly, somewhat overestimated.

(4) Boundary conditions (striker and anvil) can be well modelled with contact elements. Friction does not seem to play an important role: the friction coefficient seems to be on the order of 0.1.

Whereas most of our FEM simulations focussing on the mechanical aspects of the Charpy impact test employed a classical non-dilatant (though rate dependent) plasticity material model, the already presented rate dependent GTN model was used for local approach analysis. This has the advantage that the modification of the stress field ahead of the notch through ductile crack growth is handled in a natural way.

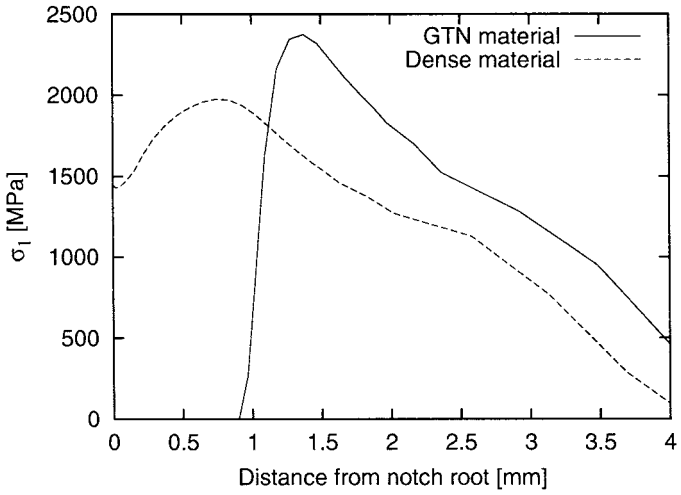

Figure 4. Comparison of the largest principal stress in the center part of the ligament ahead of the notch root of a CVN specimen, as predicted by simulation with a GTN and a dense material, for a displacement of 2.75 mm. $T = -60$ °C.

We first compare the influence of the constitutive equations on the global response. Three computed load-deflection curves are presented in Figure 3. The following material laws are compared: GTN material, Gurson material (thus without void growth acceleration due to void coalescence), and 'dense' material. A good fit with the experimental load record is obtained. Up to a deflection of about 1.3 mm, the load curves are identical whatever the material law. However, at larger deflection the load is diminished by ductile crack growth; this effect can only be captured with the GTN model.

Comparing the influence of different constitutive equations on local stress fields is of even greater importance, since the value of the maximum principal stress σ_1 enters the cleavage fracture model. No notable difference in the stress fields can be depicted between computations employing the 'porous' GTN or a 'dense' (classical non dilatant) plasticity formulation, as long as the void volume fraction (GTN model) remains below the 'critical' value f_c. The situation changes drastically, once substantial ductile crack growth has occured (Figure 4). Not only the location of the stress peak has shifted due to ductile crack advance, also the stress level is increased from 2000 MPa in the dense material to 2400 MPa in the GTN material. A reflection of this difference can also be expected in applications of the Beremin model for brittle fracture prediction.

Figure 5 illustrates the evolution of the ductile crack front as well as the change of the stress field with specimen deflection, in the part of the ligament that is loaded in tension (i.e., where fracture initiates). Compared to an actual (experimental) crack front (Figure 2), the main features of the fracture surface are correctly modelled. However, shear lips lack description in computation, and the length of the ductile crack seems slightly overestimated (last plot in Figure 5, as compared to the corresponding fracture surface shown in Figure 2). Note again that the stress increases due to ductile crack growth, and that the stress maximum contracts towards the center plane of the specimen with increasing deflection. Probably the correct description of the shear lips would not change the stress maximum drastically. In the last plot shown in Figure 5 the ductile crack tip has already reached the end of the finely

Table 2. Weibull parameters. $V_o = (100\ \mu\text{m})^3$

Specimen type	T (°C)	N	m	σ_u (MPa)	90% confidence interval for m	90% confidence interval for σ_u	$\sigma_u V_0^{1/m}$
NT2	−150	35	19.7	2879	15.6–24.7	2836–2923	2026
NT4	−90	20	59.0	1918	43.8–80.2	1905–1931	1706
CVN	−90	28	16.5	3127	12.8–21.3	3065–3191	2056
CVN	−60	27	13.1	3994	10.2–17.0	3893–4099	2359
CVN	−30	27	9.8	5752	7.6-12.7	5558–5956	2842
CT	−90	24	16.5	3115	12.6-21.8	3048–3184	2052

meshed part of the ligament, and the stress maximum has shifted far into a relatively coarsely meshed region, where its resolution is lower.

3.3. Fracture toughness prediction

Our numerical model is completed with a brittle (cleavage) fracture model (Mudry, 1982; Beremin, 1983; Mudry, 1987), which has become one of the most popular local approach models in this area. It is based on the hypothesis of a (temperature-independent) critical cleavage stress, and on weakest link theory. The failure probability P_F is given as

$$P_F = 1 - \exp\left(-\left(\frac{\sigma_W}{\sigma_u}\right)^m\right), \tag{6}$$

with σ_W the so-called 'Weibull stress'

$$\sigma_W = \sqrt[m]{\int_{V_{\text{pl}}} (\sigma_1)^m \frac{\mathrm{d}V}{V_0}}. \tag{7}$$

where σ_1 denotes the maximum principal stress (here defined as its maximum value with time), m the Weibull exponent which describes the scatter in the flaw distribution, and σ_u is closely linked to the intrinsic cleavage stress. The integral denotes the summation of σ_1 over the entire plastified volume V_{pl} of the structure (i.e., all elements that have undergone plastic deformation), since plastic deformation is a necessary precursor to slip-induced cleavage (e.g., by a dislocation pile-up mechanism). Two parameters are required: m and $V_0\sigma_u^m$.

The fracture criterion is thus based on one mechanical variable, i.e., σ_1. Fracture is assumed to occur as soon the maximal principal stress reaches a positive value that is critical for unstable propagation of a cleavage microcrack. The choice of V_0 needs to obey some rules. On one hand, V_0 has to be chosen large enough in order to allow for the presence of a critical flaw. On the other hand, V_0 needs to be small enough in order to resolve strong stress gradients, as they occur ahead of a crack tip. In 'local' FEM computations (i.e.), if no averaging over several finite elements is carried out) the size of V_0 has to be seen in relation to the mesh size. Thus the choice of the mesh size is important for ductile crack growth modelling, as mentioned above, as well as for the cleavage modelling. The element size in the direction of the strongest gradients being imposed by the necessity for appropriate 'local' ductile crack advance modelling (see previous section), V_o was chosen $(100\ \mu\text{m})^3$.

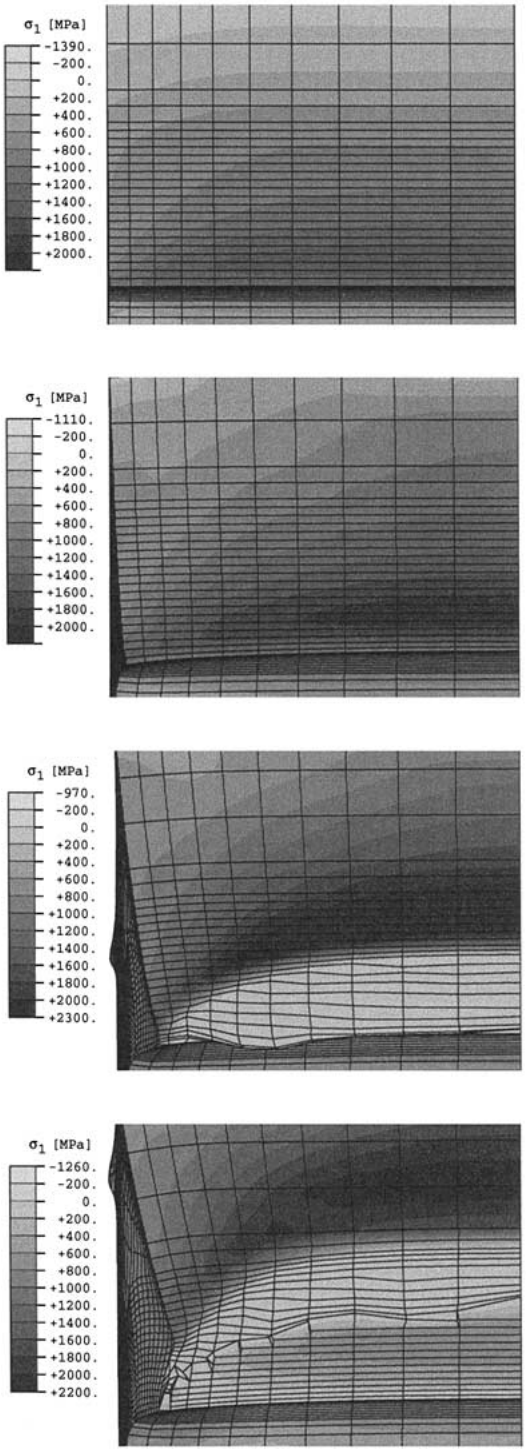

Figure 5. Contour plots of the largest principal stress in the ligament of a CVN specimen, showing its evolution with displacement d. $T = -30\ ^{\circ}\mathrm{C}$. The section shown corresponds to the area inside the white box in Figure 2. From top to bottom: $d = 0.25$ mm (roughly corresponding to the displacement at limit load); $d = 1.25$ mm; $d = 3.25$ mm; $d = 5$ mm (corresponding exactly to the deflection of the specimen shown in Figure 2; here most of the failed elements have been removed in order to prevent excessive mesh distortion.).

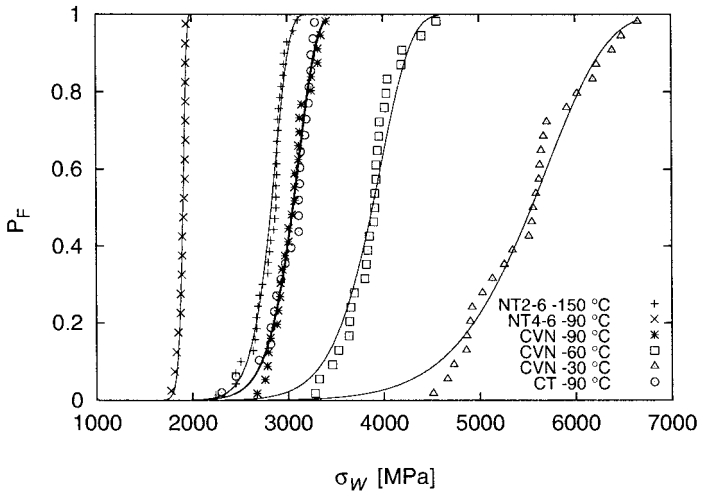

Figure 6. Weibull plots of the entire set of specimens. $V_0 = (100\ \mu\text{m})^3$. NT:notched tensile; CVN: Charpy V-notch; CT: compact tension specimens.

The two parameters m and σ_u were determined by post-processing of FEM and experimental results with the maximum likelihood method. This method leads to the narrowest confidence intervals (Khalili and Kromp, 1991) and is recommended by ESIS (1997). It should be emphasized that the comparison between quasistatic and implicit dynamic 2-D computation of the CVN specimen (for a temperature of -90 °C) yielded a practically identical evolution of the Weibull stress σ_W with time, in accordance with the previously cited observation of rapid damping of inertial stress oscillations ahead of the specimen notch root. This is another indication that quasistatic computation is sufficient in this domain.

Figure 6 and Table 2 show Weibull plots and parameters, respectively, for the entire set of specimens. Recall that the FEM computations of all specimen types incorporate ductile damage and crack growth via the GTN model. Compared to the values of the Weibull parameters identified here, similar ones have been found for similar materials in previous studies: taking $V_0 = (50\ \mu\text{m})^3$, Beremin (1983) found $m = 22$ and values for σ_u between 1970 MPa and 2800 MPa (for different heats); Tahar (1998) obtained $m = 21$ and $\sigma_u = 2809$ MPa. It is found that the Weibull plots for the CVN and CT specimens (both tested at -90 °C) are practically identical, and the smoothly notched NT2 specimen (tested at -150 °C) yields parameters that are comparable. However, the parameters calculated for the other specimen geometries differ substantionally.

If a unique set of parameters exists, the fracture toughness can also be predicted. Beremin (1983) already proposed a semi-analytical procedure that is based on the RKR model (Ritchie et al., 1973). The formulation reads

$$K_{Ic} = \left(\frac{\ln\left(\dfrac{1}{1 - P_F}\right) V_0 \sigma_u^m}{\sigma_y^{m-4} B C_m} \right)^{1/4} \tag{8}$$

and yields a link between failure probability and fracture toughness. B is the specimen thickness, and C_m a factor that is dependent on m and on the hardening behaviour of the material, and needs to be determined numerically. This semi-analytical analysis allows easy estima-

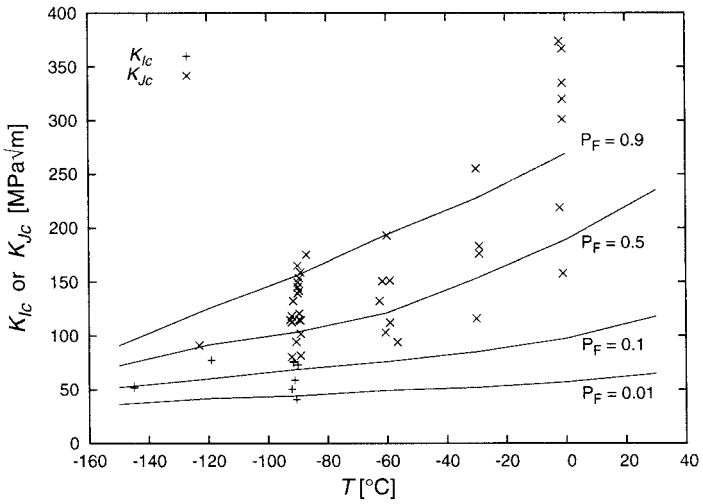

Figure 7. Fracture toughness at cleavage initiation as predicted from CVN results obtained at −90 °C. K_{Jc} denotes an equivalent fracture toughness computed from J_{Ic}. P_F is the failure probability.

tions. However, since it requires numerical computation, it is more consistent to carry out an entirely numerical analysis (e.g., by FEM), which necessites less assumptions (state of stress, material behaviour), and should thus allow higher precision.

We based our prediction on FEM analysis, as described in Section 3.1. The failure probability of the CT specimens was computed with the same FEM post-processing routine as already presented at the beginning of this section, except that the Weibull parameters are not optimised with the maximum likelihood method but imposed as those determined for the CVN specimens. At the same time, for each loading step, the J-integral was evaluated and converted into an equivalent K_I value.

Figure 7 shows the resulting prediction of fracture toughness for CT specimens, as computed with the Weibull parameters determined from the Charpy results obtained at $T = -90$ °C. These parameters being very close to those of the CT specimens (that were tested at the same temperature) one finds without surprise that the prediction of fracture toughness, *for this temperature*, is very satisfying. The prediction seems still reasonable towards lower temperature, although the scarcity of experimental results does not allow reliable verification. However, although ductile crack growth has been fully accounted for in our computation, the combined GTN-Beremin approach fails to correctly describe the ductile-to-brittle transition, if the Beremin parameters established at low temperature are kept constant. The increase with temperature of fracture toughness in the brittle-to-ductile transition is underestimated: Notably, the lower bound of fracture toughness barely increases, in contrast with experience. Thus it may be concluded that solely the evolution of the material flow stress with temperature is not sufficient in order to explain the steep rise of the material's resistance to cleavage crack growth in the brittle-to-ductile transition.

4. Discussion

A few attempts to combine the GTN and Beremin models in order to describe the ductile-to-brittle transition have already been made (Xia and Shih, 1996; Ruggieri and Dodds, Jr., 1996; Xia and Cheng, 1997; Bernauer et al., 1999). Only Bernauer et al. (1999) confront

the computations with an extensive experimental database. Their findings confirm the results of this study, i.e. that the Beremin parameters depend on the specimen geometry and test temperature. Thus the physical basis of the Beremin model must be questioned.

In order to gain more insight into the physical mechanism leading to cleavage failure, fractography may be a useful tool. As already shown in Figure 2, the macroscopic pattern of ridges that form a sort of 'fan' on the cleavage fracture surface may be traced back and, at a higher resolution, reveals a cleavage initiation site (Figure 8, – note that the specimen shown is not identical to the specimen on Figure 2).

Renevey (1997) studied the cleavage initiation sites in the notched tensile specimens tested at -150 °C and -90 °C. In most cases, a single initiation site could be identified. According to the microstructural features present, the sites were classified as follows: (1) cluster of manganese inclusions; (2) cluster of manganese inclusions and a significant amount of ductile damage; (3) other: alumina or TiC inclusions, or no microstructural feature identified. The three categories were present in specimens tested at lower temperature ($T = -150$ °C), whereas only the second category was found in specimens tested at higher temperature ($T = -90$ °C). The average size of the sites increases with temperature.

A similar fractographic study was conducted on 84 of our Charpy specimens and 38 of the CT specimens (Nedbal et al., 1997; Mäntylä et al., 1999) and yielded the following findings:

– The specimens that fractured at low temperature (in a very brittle manner) exhibit a very flat fracture surface and only rarely macroscopic cleavage 'fans'. In that case, frequently multiple cleavage initiation sites were found. The total number of cleavage initiation sites (comprising the principal and secondary sites) decreases with increasing temperature.

– The types of the principal cleavage initiation sites were defined in a slightly different manner from those defined by Renevey (1997), that is: (1) small, approximately spherical inclusion (of 2–3 μm diameter), often composed of MnS and/or oxide, or TiC; (2) large, elongated inclusion mainly composed of MnS (length on the order of 100 μm) , or cluster of large inclusions; (3) any other particular feature that was encountered in the cleavage initiation area, such as a grain boundary or a cluster of large cleavage facets (indicating abnormally large grains). Most sites were attributed to categories (1) or (2).

– The type of active cleavage initiation site is strongly determined by temperature, such that it was almost exclusively large MnS stringers in CVN specimens fractured at $T = -30$ °C (highest temperature examined). Note that Renevey's analysis of inclusions on cut sections yielded an average size of inclusions of only 10 μm, with an aspect ratio close to 1. It can be followed that at higher temperature only the tail of the size distribution of inclusions plays an active role in triggering cleavage.

– Temperature influences also the location of the cleavage initiation sites. With increasing temperature, they appear to concentrate towards the specimen mid-plane. This can be explained by increasing plastic constraint with increasing temperature in the specimen interior.

We note that failure does seem to be triggered by a weakest-link mechanism, as assumed in the Beremin model. However, the 'active' population of weak spots seems to evolve with temperature.

Further information about the physical mechanisms of damage was sought by interrupting three tests on CT specimens (with an *a/W* ratio of 0.60), at -60 °C. It was intended to pre-load the specimens to a fairly high load level (i.e., in order to assure the possibility of damage), and then interrupt the tests and carefully continue crack propagation by fatigue, in order to mark the eventual damage induced by pre-loading. Thus the potential existence of stable cleavage cracks prior to final cleavage fracture could be revealed.

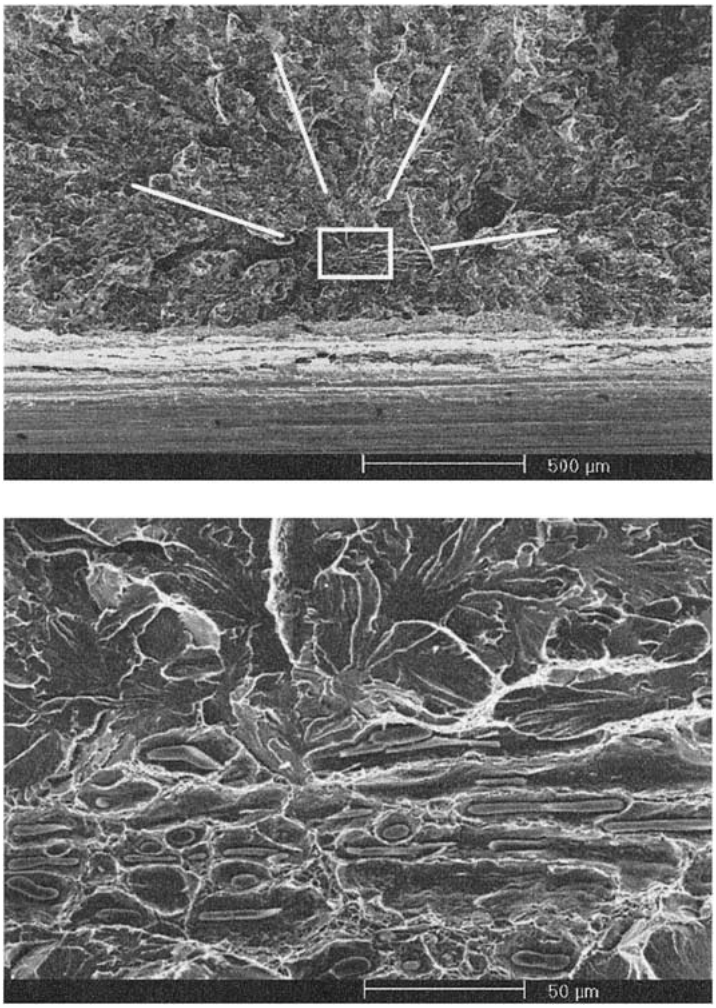

Figure 8. Principle used for tracing back the cleavage initiation site. Top: low magnification showing tear ridges starting from the center area in the photograph. Bottom: high magnification revealing a cluster of MnS inclusions that appears to have triggered cleavage.

One of the specimens failed during the pre-loading, which confirms that the load level chosen was high enough. One specimen did not show any damage but the stretch zone and fatigue damage. On the fracture surface of the third specimen, a cluster of cleavage facets can be depicted, immediately behind the stretch zone (Figure 9). Still further away a cluster of manganese sulfides is situated. One can only speculate about the exact history of events. However the following scenario seems plausible. During loading, debonding of the inclusions occurred. The strong stress concentration, in the area between the stretch zone and the crack-like void formed by inclusion debonding, induced cleavage initiation on a few grains. This cleavage crack being 'trapped' between the stretch zone and the void, it could not propagate further and was arrested.

Cleavage in structural steels is commonly considered to be initiated by dislocation pile-up or by carbide cracking. Only little evidence has been found of the possible role on cleavage fracture of larger non-metallic inclusions, e.g. manganese sulfides, whereas their role in ductile

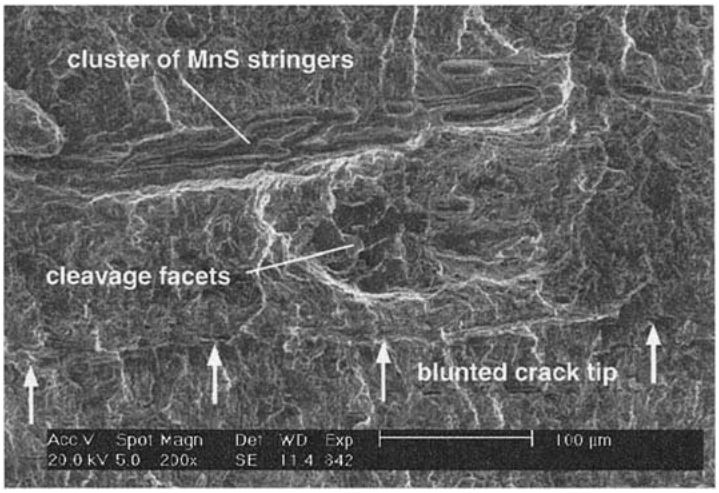

Figure 9. Fractography of a specimen that was pre-loaded to 40 kN and subsequently fractured by fatigue. On the bottom, the crack tip blunting zone can be depicted (crack growth from bottom to top of the figure). In the center, cleavage facets. On top, a cluster of MnS sulfides, that apparently favoured cleavage initiation, and subsequently prevented cleavage crack extension by 'trapping' the crack.

fracture is well documented. Tweed and Knott (1983, 1987) seem to be the first authors to report MnS inclusion induced cleavage, in a C-Mn weld metal. Subsequently, further confirmation of possible inclusion-induced cleavage fracture has been found, again for C-Mn weld metal (McRobie and Knott, 1985), for bainitic A508 or A533 pressure vessel steel (Rosenfield et al., 1983; Bowen and Knott, 1984, 1985; Miglin et al., 1990; Brückner-Foit et al., 1990; Gibson et al., 1991; Heerens et al., 1991), and for a resulphurized mild steel (Baker et al., 1986).

Several reasons can be evoked in order to explain the relative scarcity of observations of inclusion-induced cleavage initiation. Occurrence of this mechanism is evidently dependent on the presence of inclusions, on their number, size and shape, and on the specimen orientation. Furthermore, most studies published in literature were conducted at very low temperature, i.e., −196 °C, whereas we found that the frequency of observations of inclusion-induced failure increases with temperature. In 80% of our specimens, manganese sulfides are present at cleavage initiation sites.

Early debonding due to weak interfacial strength during the loading process (Ono and Yamamoto, 1981; Clough and Wadley, 1982), or during the fabrication process (Brooksbank and Andrews, 1968), will thus result in a plate-like defect. The same effect is diagnosed in the S-T orientation (Bowen and Knott, 1985). It is evident that such a defect promotes brittle failure, probably by acting *indirectly* as a cleavage initiator, i.e., by raising stresses in its vicinity.

Fractographic analysis not only provides information on the physical nature of cleavage triggering microstructural features, but also reveals their location. For each identified cleavage initiation site, the instant of specimen failure t is known, as well as the in-plane coordinates x and y (r in the case of axisymmetric specimens). Thus each site can be associated with a specific finite element in the corresponding FEM model of the specimen. The deformation of the specimen, which induces a mesh distortion, has to be taken into account, as well as the evolution of variables with time. The knowledge of the mechanical state of the material *at the*

location and instant where failure occurred may serve to establish the 'failure locus' of the material.

Figure 10 shows the local maximum principal stress at cleavage initiation, as a function of the equivalent plastic strain. At all failure locations, plastic deformation has occurred ($\epsilon_{\mathrm{pl}} > 0$). Thus the very general assumption on the role of plastic strain as a precursor for cleavage initiation is confirmed. However, note that plastic strain values cover a very large interval, ranging from as low as 0.1% to almost 50%. Stress values are also subject to a large scatter, ranging from 1200 MPa to twice as much, i.e., 2400 MPa. Even if the lowest and highest values are considered 'outliers', the interval still extends from 1400 MPa to 2300 MPa. Stress defined here is computed with the GTN model and corresponds to the stress in an 'equivalent' material (composed of dense matrix and voids). However, unless a finite element has started to fail, through reaching the critical void volume fraction f_c, which induces a drastic stress drop, porosity is low and its influence on stress is negligible. Over the entire set of specimens, three fractographic sites were found to correspond to finite elements that had already failed (all of them in CVN specimens tested at -30 °C) and thus were attributed zero stress values by our post-processing routine. This finding is explained by the irregularity of actual ductile crack fronts as compared to the deterministically computed crack progagation. The corresponding data points were not taken into account.

From Figure 10 no distinct influence of the amount of plastic strain on the apparent cleavage stress can be put into evidence. Analysis of the evolution of stress with time revealed that fracture can also be triggered when the local stress has already passed its maximum value ($\partial\sigma_1/\partial\sigma < 0$), which is in accordance with findings reported by Bernauer (1997).

Another correlation of potential interest for cleavage may be sought between the cleavage stress and stress triaxiality (Figure 11). Especially for cracked specimens (CT and CVN tested at $T = -30$ °C), the stress rise induced by increasing triaxiality can be clearly depicted. Triaxiality is increased in CVN specimens by ductile crack initiation. However, the large range of triaxiality values that occur at sites of cleavage initiation in specimens of different geometry is again not conclusive with respect to the necessity of incorporating a triaxiality criterion into a cleavage fracture model. We also studied correlations with other variables and did not detect any clear trend.

Nevertheless, an interesting tendency can be depicted in Figure 12. In Charpy specimens, for which results are available over a larger range of temperatures than for any other specimen geometry, the cleavage stress increases roughly linearly with temperature. This result is in agreement with the already presented observation of the increase in size of cleavage initiation sites with temperature. If one postulates that the material's intrinsic resistance to cleavage fracture increases with temperature (at least in the brittle-to-ductile domain), the critical flaw size has to evolve as well. However, the physical soundness of the assumption of a temperature-dependent cleavage stress is still questionable. In any case, for each studied temperature, the scatter of stress values is quite low, such that the critical role of stress on cleavage fracture is confirmed.

In view of the discussion above, the breakdown of the Beremin model to cover a large temperature range, notably in the transition region, is not surprising, since the cleavage stress is assumed temperature independent in the present formulation. In order to increase the stability of the Beremin model, propositions for modification have already been made. However, they are generally not based on the assumption of an evolution of the cleavage stress with temperature.

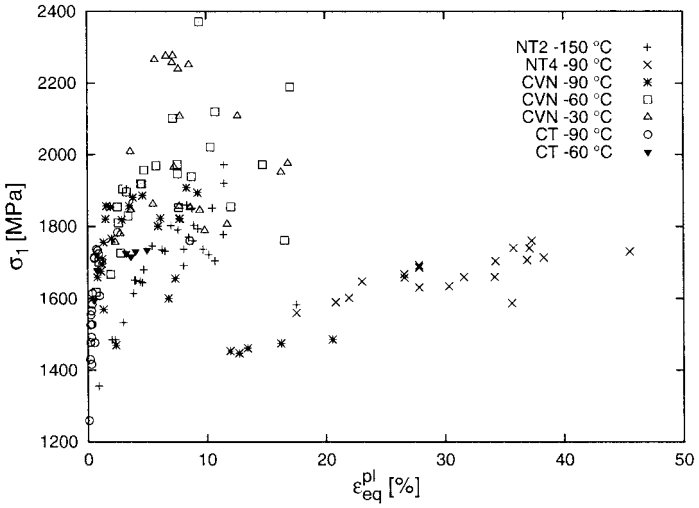

Figure 10. Local value of the cleavage stress (largest principal stress at the cleavage site) vs. equivalent plastic strain for the entire set of specimens analysed in fractography. NT: notched tensile; CVN: Charpy V-notch; CT: compact tension specimens.

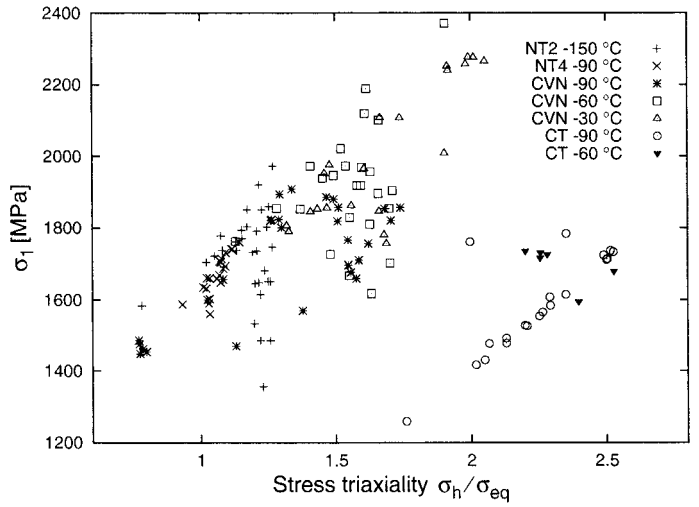

Figure 11. Local values of the cleavage stress (largest principal stress at the cleavage site) vs. stress triaxiality $\sigma_h/\sigma_{\text{eq}}$ for the entire set of specimens analysed in fractography. NT: notched tensile; CVN: Charpy V -notch; CT: compact tension specimens.

A first proposition was already made by Beremin (1983) in form of a strain-correction, applied to specimens that had been pre-strained. We tentatively applied this correction in our study and did not state any improvement (Rossoll, 1998).

Chen et al. (1996) introduced additional triaxiality and strain criteria, i.e., minimum values for these variables. However, their study is based exclusively on pre-cracked specimens, which severely restricts the transferability of this model. furthermore, in pre-cracked specimens triaxiality is always high, whereas our experimental data show (Figure 11) that cleavage may be triggered also on low constraint situations, as has already been stated above. Thus such a modification does not appear to be justified.

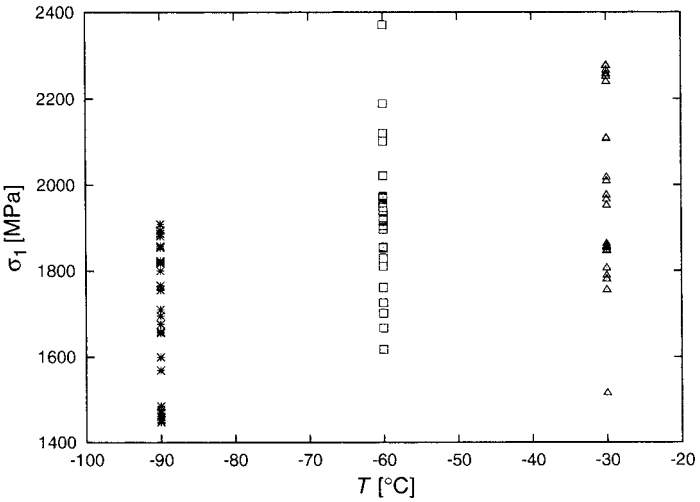

Figure 12. Local values of the cleavage stress (largest principal stress at the cleavage site) vs. temperature (only Charpy specimens).

Xia and Shih (1996) propose the correction of the expression for the Weibull stress (Equation (7) by a term that reduces σ_W by the probability of void nucleation, i.e., under the hypothesis that cleavage cannot be initiated, once ductile damage has occurred. Actually this correction would make the Weibull stress evolve slower in the case of the CVN specimens tested at the temperatures -60 °C and 30°C, and probably bring the Weibull parameters of most of the different specimen geometries closer together. However, the idea behind this model is in contradiction with our experimental observations, since ductile damage was found to be a major factor for cleavage initiation in the transition domain, in our material.

Bernauer et al. (1999) tested a similar modification, and actually found that the values of σ_u lie in a closer interval (notably if a constant m of 30 is imposed). However, parameters were still not unique. Another modification that was also tested by these authors is based on the decrease of microcrack formation with plastic strain. This model yielded no improvement concerning the transferability of parameters. Other approaches (Renevey, 1997) consider a coupling of 'pure' cleavage and ductile fracture probabilities, or account for the initiation of cleavage from clusters of inclusions. However, these models did not seem to apply to different specimen geometries and temperatures as well.

For the material of our study, besides the open question of a temperature dependence of the cleavage stress, an important question is how the presence of 'macroscopic' flaws (clusters of inclusions) can be properly accounted for. If the concept of a fully-coupled ductile-brittle analysis is followed (e.g., with the GTN model), ductile crack initiation would need to be modelled as spatially heterogeneous, which makes the practical application of such an approach extremely labourous. On the other hand, if the 'macroscopic' flaws are considered as 'weak spots' (capable of triggering cleavage fracture in their vicinity) in an otherwise homogeneous material, the parameter V_0 would need to reflect the size of such flaws. Since the average size of these flaws was found to evolve with temperature, V_0 would need to evolve as well. Besides the difficulty of defining such a functionality, strong stress gradients (notably ahead of a crack tip) would be present in large volumes V_0, which violates the weakest link concept. Thus it seems that any attempt of physically motivated modification of the Beremin model is difficult to achieve in practice.

5. Conclusions

The feasibility of lower-shelf fracture toughness determination by means of the Charpy impact test was shown. The local approach method was chosen, which combines a physically-based model of fracture (whose parameters are phenomenologically determined) with FEM modelling. It is an *a priori* geometry independent scheme that does not require the use of pre-cracked specimens. The dynamic effects in the Charpy test were accounted for with a rate dependent formulation of the material flow stress and the incorporation of adiabatic heating, whereas inertial terms were found negligible. The modification of the stress fields by ductile crack growth were fully incorporated with the GTN model.

The Beremin model seems to yield consistent parameters in CVN and CT specimens as long as one specific temperature (on the lower of fracture toughness) is considered. In this domain, fracture toughness can be predicted. The weakest link hypothesis that serves as a basis of this model is confirmed by a fractographic analysis which indicates cleavage initiation from a principal site acting as a weak spot. In the tested material, cleavage fracture was frequently triggered by inclusions.

Towards the brittle-to-ductile transition, some changes take place. Fractographic analysis reveals a change of the population of cleavage triggering inclusions to larger sizes. Correlation of the cleavage initiation sites with FEM analysis shows that the local cleavage stress also increases with temperature. It is postulated that the intrinsic resistance to cleavage crack initiation increases with temperature, which would also to be expected in material where cleavage is not triggered by inclusions (e.g., different specimen orientation). The incorporation of this assumption into the Beremin model calls also for a concomitant increase of the characteristic volume, which seems difficult to model in practice.

Acknowledgements

We thank EdF (Les Renardières) for financial support and for supplying the material. CEA/CEREM/SRMA (Saclay) is acknowledged for the interesting and fruitful collaboration. A. Rossoll is grateful to the European Commission (DG XII -DEMA) for financial support under contract number FI4S-CT96-5001.

References

Ayres, D. (1976). Dynamic plastic analysis of ductile fracture–the Charpy specimen. *International Journal of Fracture* **12**, 567–78.

Baker, T., Kavishe, F. and Wilson, J. (1986). Effect of non-metallic inclusions on cleavage fracture. *Materials Science and Technology* **2**, 576–582.

Barsom, J. (1975). Development of the AASHTO fracture-toughness requirements for bridge steels. *Engineering Fracture Mechanics* **7**, 605–618.

Barsom, J. and Rolfe, S. (1970). Correlations between K_{Ic} and Charpy V-notch test results in the transition temperature range. In: *Impact Testing of Metals, ASTM STP 466*. Philadelphia, USA, 281–302.

Beremin, F. (1983). A local criterion for cleavage fracture of a nuclear pressure vessel steel. *Metallurgical Transactions A* **14A**, 2277–2287.

Bernauer, G. (1997). Einsatz mikromechanischer Schädigungsmodelle im sprödduktilen Ubergangsbereich. Ph.D. thesis, Universität Karlsruhe, Germany. Also IWM Report W 5/97, Freiburg, Germany.

Bernauer, G., Brocks, W. and Schmitt, W. (1999). Modifications of the Beremin model for cleavage fracture in the transition region of a ferritic steel. *Engineering Fracture Mechanics* **64**, 305–325.

Bodner, S. and Symonds, P. (1960). Plastic deformations in impact and impulsive loading of beams. In: *Plasticity. Proceedings of the Second Symposium on Naval Structural Mechanics.* (Edited by Lee, E. and Symonds, P.) Rhode Island, USA, pp. 488–500.

Bowen, P. and Knott, J. (1984). Cleavage fracture of A 533 B pressure vessel steel in martensitic condition. *Metal Science* **18**, 225–235.

Bowen, P. and Knott, J. (1985). Some observations on the assessment of short, sharp cracks at the roots of blunt notches, and their effect on brittle fracture. *International Journal of Fracture* **28**, 103–117.

Brooksbank, D. and Andrews, K. (1968). Thermal expansion of some inclusions found in steels and relation to tessellated stresses. *Journal of the Iron and Steel Institute* **206**, 595–599.

Brückner-Foit, A., Ehl, W., Munz, D. and Trolldenier, B. (1990). The size effect of microstructural implications of the weakest link model. *Fatigue & Fracture of Engineering Materials & Structures* **13**, 185–200.

Chen, J., Wang, G. and Wang, H. (1996). A statistical model for cleavage fracture of low alloy steel. *Acta Materialia* **44**(10), 3979–3989.

Chu, C. and Needleman, A. (1980). Void nucleation effects in biaxially stretched sheets. *Journal of Engineering Materials and Technology* **102**, 249–256.

Clough, R. and Wadley, H. (1982). Indentation loading pudies of acoustic emission from temper and hydrogen embrittled A533B steel. *Metallurgical Transactions* **13A**, 1965–1975.

ESIS: 1996a, Proposed standard methods for instrumented pre-cracked Charpy impact testing of steels. European Structural Integrity Society, TC5. Draft 10.

ESIS: 1996b, Proposed standard methods for instrumented pre-cracked Charpy impact testing of steels. Combined K_{Id}, J_{Id} and CTOD methods. European Structural Integrity Society, TC5. Draft 6.

ESIS: 1997, Draft procedure to measure and calculate local approach criteria using notched tensile specimens. European Structural Integrity Society, TC 1.1. Draft document (v 4.0).

Fearnehough, G. and Hoy, C. (1964). Mechanism of deformation and fracture in the Charpy test as revealed by dynamic recording of impact loads. *Journal of the Iron and Steel Institute* 912–920.

Fisher, J. and Gurland, J. (1981). Void nucleation in spheroidized carbon steels. Part 1: Experimental. *Metal Science* **15**, 185–192.

Franklin, A. (1969). Comparison between a quantitative microscope and chemical methods for assessment of non-metallic inclusions. *Journal of The Iron and Steel Institute*, 181–186.

Gibson, G., Capel, M. and Druce, S. (1991). Effect of heat treatment on the fracture toughness transition properties of an A508 class 3 steel. In: *Defect Assessment in Components–Fundamentals and applications*. (edited by: Blauel, J. and Schwalbe, K.-H.) ESIS/EGF Publication 9, 587–611.

Gurson, A. (1977). Continuum theory of ductile rupture by void nucleation and growth: Part I – Yield criteria and flow rules for porous ductile media. *Journal of Engineering Materials and Technology*, 2–15.

Heerens, J., Read, D., Cornec, A. and Schwalbe, K.-H. (1991). Interpretation of fracture toughness in the ductile-to-brittle transition region by fractographical observations. In: *Defect Assessment in Components – Fundamentals and Applications.* (edited by Blauel, J. and Schwalbe K.-H.), ESIS/EGF Publication 9, 659–678.

Hertzberg, R. (1995). *Deformation and Fracture Mechanics of Engineering Materials,* pp. 390–399. New York (USA): J. Wiley, 4th edition.

HKS: (1997). ABAQUS / Standard, Version 5.7, Theory Manual. Hibbitt, Karlsson & Sorensen, Inc., Pawtucket, RI, U.S.A.

Khalili, A. and Kromp, K. (1991). Statistical properties of Weibull estimators. *Journal of Materials Science* **26**, 6741–6752.

Knott, J. (1967). On stress intensifications in specimens of Charpy geometry prior to general yield. *Journal of the Mechanics and Physics of Solids* **15**, 97–103.

Kwon, D. and Asaro, R. (1990). A study of void nucleation, growth, and coalescence in spheroidized 1518 steel. *Metallurgical Transactions A* **21A**, 117–134.

Mäntylä, M., Rossoll, A., Nedbal, I., Prioul, C. and Marini, B. (1999). Fractographic observations of cleavage fracture initiation in a bainitic A508 steel. *Journal of Nuclear Materials* **264**, 257–262.

Marandet, B. and Sanz, G. (1977). Evaluation of the toughness of thick medium-strength steels by using linear-elastic fracture mechanics and correlations between K_{Ic} and Charpy V-notch. In: *Flaw Growth and Fracture, ASTM STP 631.* Philadelphia, USA, pp. 72–95.

Marur, P. (1996). Numerical simulation of anvil interactions in the impact testing of notched bend specimens. *International Journal of Fracture* **81**, 27–37.

Mathur, K., Needleman, A. and Tvergaard, V. (1993). Dynamic 3D analysis of the Charpy impact test. *Modelling and Simulation in Materials Science and Engineering* **1**, 467–484.

McRobie, D. and Knott, J. (1985). Effects of strain and strain aging on fracture toughness of C-Mn weld metal. *Materials Science and Technology* **1**, 357–365.

Miglin, M., Wade, C. and Van Der Sluys, W. (1990). Analysis of fracture toughness data for modified SA508 Cl2 in the ductile-to-brittle transition region. In: *Fracture Mechanics: Twenty-First Symposion, ASTM STP 1074*. (Edited by: Gudas, J., Joyce, J. and Hackett, E.), Philadelphia, U.S.A., 238–263.

Mudry, F. (1982). Etude de la rupture ductile et de la rupture par clivage d'aciers faiblement alliés. Ph.D. thesis, Université de Technologie de Compiègne.

Mudry, F. (1987). A local approach to cleavage fracture. *Nuclear Engineering and Design* **105**, 65–76.

Mühlich, U., Siegmund, T. and Brocks, W. (1998). A User-Material Subroutine of the Gurson-Tvergaard-Needleman Model of Porous Metal Plasticity for Rate and Temperature Dependent Hardening. Technical Note GKSS/WMG/98/1, GKSS, Geesthacht, Germany.

Nakamura, T., Shih, C. and Freund, L. (1989). Three-dimensional transient analysis of a dynamically loaded three-point-bend ductile fracture specimen. In: *Nonlinear Fracture Mechanics: Volume I-Time-Dependent Fracture, ASTM STP 995*. (Edited by: Saxena, A., Landes, J. and Bassani, J.) Philadelphia, U.S.A., 217–241.

Nedbal, I., Siegl, J. and Kunz, J. (1997). Ductile Initiation of Cleavage in Charpy V-Notch Specimens of Bainitic Steel A508 Cl.3. Research Report V-KMAT-440/97, CVUT-FJFI-KMAT, Prague, Czech Republic.

Norris, Jr., D. (1979). Computer simulation of the Charpy V-notch toughness test. *Engineering Fracture Mechanics* **11**, 261–274.

Ono, K. and Yamamoto, M. (1981). Anisotropic mechanical and acoustic emission behavior of A533B steels. *Materials Science Engineering* **47**, 247–263.

Perzyna, P. (1963). The constitutive equations for rate sensitive plastic materials. *Quarterly of Applied Mathematics* **20**(4), 321–332.

Renevey, S. (1997). Approches globale et locale de la rupture dans le domaine de transition fragile-ductile d'un acier faiblement allié. Ph.D. thesis, Université Paris XI Orsay, France.

Ritchie, R., Knott, J. and Rice, J. (1973). On the relationship between critical tensile stress and fracture toughness in mild steel. *Journal of the Mechanics and Physics of Solids* **21**, 395–410.

Rosenfield, A., Shetty, D. and Skidmore, A. (1983). Fractographic observations of cleavage initiation in the ductile-brittle transition region of a nuclear reactor-pressure-vessel steel. *Metallurgical Transactions* **14A**, 1934–1937.

Rossoll, A. (1998). Détermination de la ténacité d'un acier faiblement allié à partir de l'essai Charpy instrumenté. Ph.D. thesis, École Centrale de Paris, France. In English.

Rossoll, A., Berdin, C., Forget, P., Prioul, C. and Marini, B. (1999). Mechanical aspects of the Charpy impact test. *Nuclear Engineering and Design* **188**, 217–229.

Ruggieri, C. and Dodds, R., Jr. (1996). A transferability model for brittle fracture including constraint and ductile tearing effects: a probabilistic approach. *International Journal of Fracture* **79**, 309–340.

Sailors, R. and Corten, H. (1972). Relationship between material fracture toughness using fracture mechanics and transition temperature tests. In: *Fracture Toughness, Proceedings of the 1971 National Symposion on Fracture Mechanics, Part II, ASTM STP 514*. Philadelphia, U.S.A., pp. 164–191.

Server, W. (1978a). General yielding of Charpy V-notch and precracked specimens. *Journal of Engineering Material and Technology* **100**, 183–188.

Server, W. (1978b). Impact three-point bend testing for notched and precracked specimens. *Journal of Testing and Evaluation* **6**, 29–34.

Server, A. (1985). Charpy Impact Testing. In: *ASM Handbook*, Vol. 8. American Society for Metals pp. 261–268.

Siegmund, T. and Brocks, W. (1997). *A User-Material Subroutine Incorporating the Gurson-Tvergaard-Needleman Model of Porous Metal Plasticity into the ABAQUS Finite Element Program*. Technical Note GKSS/WMG/97/2, GKSS, Geesthacht, Germany.

Tahar, M. (1998). Applications de l'approche locale de la rupture fragile a l'acier 16MND5: - Corrélation résilience-ténacité. - Probabilité de rupture bimodale (clivage et intergranulaire). Ph.D. thesis, Ecole Nationale Supérieure des Mines de Paris, France.

Tvergaard, V. (1981). Influence of voids on shear band instabilities under plane strain conditions. *International Journal of Fracture* **17**, 381–388.

Tvergaard, V. (1982). On localization in ductile materials containing spherical voids. *International Journal of Fracture* **18**, 237–252.

Tvergaard, V. and Needleman, A. (1984). Analysis of the cup-cone fracture in a round tensile bar. *Acta Metallurgica* **32** 157–169.

Tvergaard, V. and Needleman, A. (1988). An analysis of the temperature and rate dependence of Charpy V-notch energies for a high nitrogen steel. *International Journal of Fracture 37*, 197–215.

Tweed, J. and Knott, J. (1983). Effect of reheating on microstructure and toughness of C-Mn weld metal. *Metal Science* **17**, 45–54.

Tweed, J. and Knott, J. (1987). Micromechanics of failure in C-Mn weld metals. *Acta Metallurgica* **35**, 1401–1414.

Wallin, K. (1989). A simple theoretical Charpy- V–K_{Ic} correlation for irradiation embrittlement. In: *Innovative Approaches to Irridiation Damage and Fracture Analysis*, Vol. 170 of *PVP*. (Edited by: Marriot, D., Mager, T. and Bamford, W.) 93–100.

Wilshaw, T. and Pratt, P. (1966). On the plastic deformation of Charpy specimens prior to general yield. *Journal of the Mechanics and Physics of Solids* **14**, 7–21.

Wullaert, R. (1970). Applications of the instrumented Charpy impact test. In: *Impact Testing of Metals, ASTM STP 466*. Philadelphia, U.S.A., 148–164.

Xia, L. and Cheng, L. (1997). Transition from ductile tearing to cleavage fracture: a cell model approach. *International Journal of Fracture* **87**, 289–306.

Xia, L. and Shih, C. (1996). Ductile crack growth–III. Transition to cleavage fracture incorporating statistics. *Journal of the Mechanics and Physics of Solids* **44**, 603–639.